# Microscopic molecular dynamics characterization of the second-order non-Navier-Fourier constitutive laws in the Poiseuille gas flow

A. Rana,[1] R. Ravichandran,[1] J. H. Park,[1,2] and R. S. Myong[1,2,a)]
[1]*School of Mechanical and Aerospace Engineering, Gyeongsang National University, Jinju, Gyeongnam 52828, South Korea*
[2]*Research Center for Aircraft Parts Technology, Gyeongsang National University, Jinju, Gyeongnam 52828, South Korea*

(Received 23 April 2016; accepted 10 July 2016; published online 1 August 2016)

The second-order non-Navier-Fourier constitutive laws, expressed in a compact *algebraic* mathematical form, were validated for the force-driven Poiseuille gas flow by the deterministic *atomic-level microscopic* molecular dynamics (MD). Emphasis is placed on how completely different methods (a *second-order continuum macroscopic* theory based on the kinetic Boltzmann equation, the *probabilistic mesoscopic* direct simulation Monte Carlo, and, in particular, the *deterministic microscopic* MD) describe the non-classical physics, and whether the second-order non-Navier-Fourier constitutive laws derived from the continuum theory can be validated using MD solutions for the viscous stress and heat flux calculated directly from the molecular data using the statistical method. Peculiar behaviors (non-uniform tangent pressure profile and exotic instantaneous heat conduction from cold to hot [R. S. Myong, "A full analytical solution for the force-driven compressible Poiseuille gas flow based on a nonlinear coupled constitutive relation," Phys. Fluids **23**(1), 012002 (2011)]) were re-examined using atomic-level MD results. It was shown that all three results were in strong qualitative agreement with each other, implying that the second-order non-Navier-Fourier laws are indeed physically legitimate in the transition regime. Furthermore, it was shown that the non-Navier-Fourier constitutive laws are essential for describing non-zero normal stress and tangential heat flux, while the classical and non-classical laws remain similar for shear stress and normal heat flux. *Published by AIP Publishing.* [http://dx.doi.org/10.1063/1.4959202]

## I. INTRODUCTION

The study of the flow and thermal characteristics of gases in rarefied and micro- and nano-scale conditions remains a fundamental topic in various disciplines.[1–11] Previous studies have revealed that the fundamental physics in conditions far from thermal equilibrium is significantly different from the classical physics governed by the linear constitutive laws that are valid in conventional flows near equilibrium. For instance, it was shown that the classical Navier[12] and Fourier[13] laws cannot predict the peculiar flow physics of the force-driven Poiseuille gas flow,[5–11] in particular, the monotonic non-uniform tangent pressure profile and non-vanishing normal stress and tangential heat flux. This indicates that the situation cannot be corrected by simply modifying the classical Navier and Fourier laws through transport coefficients, or by introducing velocity-slip and temperature-jump boundary conditions alone. It essentially demands a completely new development of the non-classical second-order theory.

In working towards this goal, which is independent of the previous high-order continuum theories, a non-classical theory based on an *algebraic* nonlinear coupled constitutive relation (called

a)Author to whom correspondence should be addressed. Electronic mail: myong@gnu.ac.kr. Tel.: +82-55-772-1645. Fax: 1580.

NCCR hereafter) was developed recently by Myong.[10,14,15] The NCCR theory was developed from the viewpoint of the moment method applied to the kinetic Boltzmann equation and the so-called (second-order) *balanced* closure.[14] The basic tenet of the NCCR theory is built on the critical observation that the number of places for closing the moment equations is two, rather than one, as misleadingly described by the previous theory based on the Maxwellian molecule assumption. Accordingly, the order of approximations in handling two terms—kinematic (movement) and dissipation (collision) terms—must be the same, for instance, second-order for both terms. Otherwise, in the case of high Mach number shock structure, the kinematic (stress-strain) coupling term of quadratic nature will grow far faster than the strain rate term, due to the destructive interplay, resulting in an imbalance with the first-order dissipation term, and eventually, a blow-up mathematical singularity.

As a result of the new closure, a second-order implicit NCCR form of the stress tensor $\mathbf{\Pi}$ and the heat flux vector $\mathbf{Q}$ was derived,[10,14,16,17]

$$\begin{aligned}
&\rho\frac{D(\mathbf{\Pi}/\rho)}{Dt} + 2[\mathbf{\Pi}\cdot\nabla\mathbf{u}]^{(2)} + 2p[\nabla\mathbf{u}]^{(2)} = -\frac{p}{\eta}\mathbf{\Pi}q_{2nd}(\kappa),\\
&\rho\frac{D(\mathbf{Q}/\rho)}{Dt} + \frac{D\mathbf{u}}{Dt}\cdot\mathbf{\Pi} - \mathbf{a}\cdot\mathbf{\Pi} + \mathbf{Q}\cdot\nabla\mathbf{u} + \mathbf{\Pi}\cdot C_p\nabla T + pC_p\nabla T = -\frac{pC_p}{k}\mathbf{Q}q_{2nd}(\kappa).
\end{aligned} \tag{1}$$

Here the second-order dissipation term, $q_{2nd}$, and the first cumulant expansion term, $\kappa$, are given in terms of the hyperbolic sine form and a Rayleigh dissipation function, respectively,

$$q_{2nd}(\kappa) = \frac{\sinh\kappa}{\kappa},\ \kappa = \frac{(mk_B)^{1/4}}{\sqrt{2}d}\frac{T^{1/4}}{p}\left(\frac{\mathbf{\Pi}:\mathbf{\Pi}}{2\eta} + \frac{\mathbf{Q}\cdot\mathbf{Q}}{kT}\right)^{1/2}.$$

In these expressions, $\rho, p, T, \mathbf{u}, \mathbf{a}$, and $D/Dt$ denote the density, the pressure, the temperature, the average velocity vector, the external force vector, and the material time derivative, respectively. $\eta$ and $k$ represent the linear (Navier) viscosity and the linear (Fourier) thermal conductivity, respectively. The $d$, $m$, and $k_B$ denote the diameter of the molecule, the molecular mass, and the Boltzmann constant, respectively. The symbol $[\ ]^{(2)}$ stands for a traceless symmetric part of the tensor and $C_p$ represents the heat capacity per unit mass at constant pressure. Note that a new term $\mathbf{a}\cdot\mathbf{\Pi}$ associated with the external force appears in the constitutive equation of heat flux in (1).

The sinh dissipation term in the second-order constitutive equation (1) originates from the Boltzmann collision integral, in which the net change in the number of gas molecules is basically described by gain minus loss, that is, $\exp^{(\text{nonequilibrium})} - \exp^{(-\text{nonequilibrium})}$, so that the leading term of dissipation next to the first-order becomes "sinh." Since the sinh term is derived through the balanced closure,[14] it guarantees the correct asymptotic free-molecular limit in all situations, including the high Mach number compressive gas flow. Interestingly, it turned out to play a minor role in the cases of velocity shear and expansive flows, since the second-order dissipation effects were cancelled under the constraint of asymptotic free-molecular behavior.[14] Notice also that the second-order NCCR model (1) reduces to the first-order linear Navier-Stokes and Fourier (simply called NSF hereafter) laws near equilibrium,[12,13]

$$\mathbf{\Pi}_0 = -2\eta[\nabla\mathbf{u}]^{(2)},\ \mathbf{Q}_0 = -k\nabla T. \tag{2}$$

When the following non-classical second-order non-Navier and non-Fourier constitutive laws (called non-Navier-Fourier laws hereafter) embodied in partial differential equation (1), expressed as a compact *algebraic* mathematical form in the case of the steady-state shear flow,[10,14]

$$\begin{aligned}
\Pi_{xy}q_{2nd}(\kappa) &= \left(1 + \frac{\Pi_{yy}}{p}\right)\Pi_{xy_0},\\
\Pi_{xy}^2 &= -\frac{3}{2}\left(p + \Pi_{yy}\right)\Pi_{yy},
\end{aligned} \tag{3}$$

$$\begin{aligned}
Q_y q_{2nd}(\kappa) &= \left(1 + \frac{\Pi_{yy}}{p}\right)Q_{y_0} + \frac{ak}{pC_p}\Pi_{xy},\\
\frac{Q_x}{Q_y} &= \frac{\Pi_{xy}Q_{y_0} + Q_y\Pi_{xy_0}/\Pr - 2ak\Pi_{yy}/C_p}{\left(p + \Pi_{yy}\right)Q_{y_0} + ak\Pi_{xy}/C_p},
\end{aligned} \tag{4}$$

respectively, were incorporated to the force-driven Poiseuille flow[10] and the Knudsen layer in Couette flow[15] in transitional regimes, the NCCR theory was shown to capture all flow peculiarities, in strong agreement with DSMC (direct simulation Monte Carlo). After additionally developing a new mathematical technique for rigorously taking into account temperature variation of transport coefficients, the new theory unraveled not only the abnormal behaviors unique to the force-driven Poiseuille flow, like monotonic non-uniform pressure profile, but also the unsolved properties in the Knudsen layer, like the velocity gradient singularity and higher central temperature.

Encouraged by these developments, we attempt in this study to validate the non-classical second-order non-Navier-Fourier constitutive laws (3) and (4) deduced from the second-order exact consequence of Boltzmann equation (1) by running a deterministic atomic-level microscopic molecular dynamics (MD) simulation for the compressible force-driven Poiseuille gas flow. Since special conditions are associated with rarefied and micro- and nano-scale gases, experimental observations that rely on the application of classical models are difficult to obtain, and this makes molecular based simulations extremely important.

MD simulation of the force-driven Poiseuille flow was performed with soft-sphere potentials by Hannon *et al*.[18] The simulation results were shown to be in agreement with hydrodynamic equations for velocity and shear-stress profiles, but with less correlation for temperature profile. The substantial gap with the classical quartic temperature profile, which may be a sign of the presence of temperature minimum at the center, was attributed to boundary contamination and temperature fluctuations, rather than the generic non-Fourier law observed in transitional regimes. Bhattacharya and Lie[19] also studied the heat and momentum transport phenomena in very dilute gases of the force-driven Poiseuille flow through MD simulations. They showed that the viscosity of a very dilute gas decreases monotonically with decreasing density, implying the shear-thinning non-Navier law in the flow. Later Todd and Evans[20] investigated the temperature profiles by carrying out MD simulations of planar Poiseuille flow between parallel isothermal atomic walls. They found the quadratic temperature profile near the center of the channel and attributed such abnormal behavior to the additional heat flux, which is proportional to the gradient of the square of the strain rate.

However, most previous MD studies had the inherent limitation of MD by itself being more akin to a computational experiment than theory, being in the class of the state-of-the-art computer simulations, and were attempts to provide a snapshot answer to the question of where the classical transport theory, based on the first-order Chapman-Enskog theory, may break down. Also, to the best knowledge of the authors, no results of the pressure and non-conserved variables (in particular, normal viscous stress and tangential heat flux), all of which are critical in validating the non-classical second-order non-Navier-Fourier constitutive laws, have been reported in previous MD studies. Further, since the first-order NSF theory limited to the linear regime was employed to guide molecular characterization of gases in the transition regime in previous MD studies, the present, more accurate second-order NCCR theory is expected to enhance molecular characterization of gases significantly.

In this study, we aim to validate the second-order holistic non-Navier-Fourier constitutive laws (3) and (4) by the most fundamental method, deterministic atomic-level microscopic MD. The analytical holistic NCCR solutions to the compressible force-driven Poiseuille flow are first summarized in Section II for further study. An explanation of the present MD simulation setup then follows in Section III. Further, the MD results of non-conserved variables, in particular, the normal viscous stress, and tangential heat flux, were calculated directly from the molecular data using the statistical method and they were illustrated in Figs. 4, 8, 10-12, 14, and 16. Finally, on the basis of non-conserved MD data, complete molecular dynamics characterization of the non-Navier-Fourier laws is achieved in Section IV.

## II. ANALYTICAL SECOND-ORDER BOLTZMANN SOLUTIONS TO THE FORCE-DRIVEN POISEUILLE GAS FLOW

The force-driven compressible Poiseuille flow is defined as a stationary flow in a channel generated by the action of a uniform external force parallel to the walls. As illustrated in Fig. 1, the flow between two infinitely separated reservoirs maintained at the same pressure and temperature

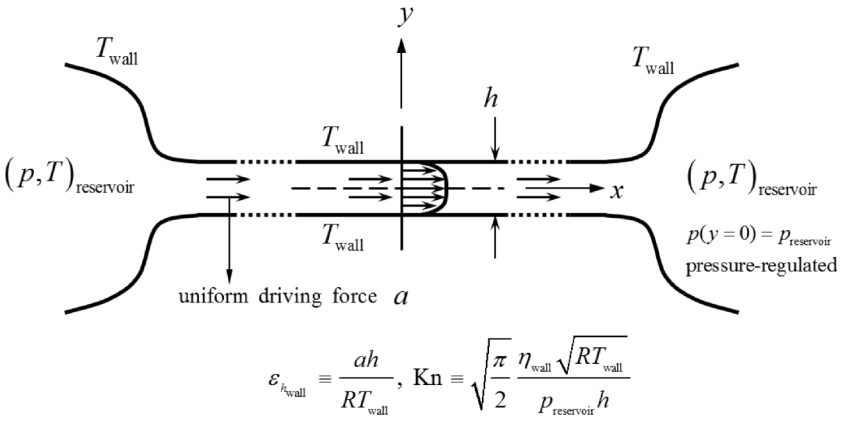


FIG. 1. A schematic diagram of the one-dimensional compressible Poiseuille gas flow in the rectangular channel (driven by a uniform force) between two *pressure-regulated* reservoirs. (Reproduced with permission from, "A full analytical solution for the force-driven compressible Poiseuille gas flow based on a nonlinear coupled constitutive relation," Phys. Fluids **23**(1), 012002 (2011). Copyright 2011 AIP Publishing LLC).

by adjusting the density can be defined uniquely by two non-dimensional parameters: the Knudsen number based on pressure (Kn) and a new parameter $\varepsilon_{h_w}$ (similar to Richardson number) on the external force. The definition of the force parameter is given by

$$\varepsilon_{h_w} = \frac{ah}{RT_w}, \tag{5}$$

where $a$ is the external force which drives the flow, $h$ is the channel height, $R$ is the gas constant for a monatomic gas, and $T_w$ is the wall temperature. The same parameter can be defined in both MD and NCCR calculations.

On the other hand, the Knudsen number in this pressure-regulated case can be defined for NCCR as

$$\mathrm{Kn} = \sqrt{\frac{\pi}{2}} \frac{\eta_w \sqrt{RT_w}}{p_m h}, \tag{6}$$

where $\eta_w$ is the viscosity at the wall temperature and $p_m$ is the pressure at the middle of the channel, and will be maintained to be the same as that of the reservoir. In the case of MD and DSMC, the Knudsen number can be defined as

$$\mathrm{Kn} = \frac{1}{\sqrt{2}\pi n d^2 h}, \tag{7}$$

where $n$ and $d$ represent the number density and the diameter of the molecule.

The analytical solutions to the conservation laws and the second-order constitutive equations for the force-driven Poiseuille gas flow have been derived for Maxwellian molecules by Myong.[10] A mathematical technique based on the average quantities for velocity and temperature profiles, a spatial variable scaled by the temperature, and subsequent auxiliary relations played a critical role in the derivation. It was also proved that a unique flow solution exists for all the physical conditions specified in terms of the Knudsen number and the force parameter. Some important solutions are summarized here for further study. (The detailed derivation of the analytical solutions and an associated code are available in the work of Myong.[10])

The NCCR solution for velocity profile is basically given as trigonometric function, in a non-dimensional form ($N_\delta = \sqrt{2\gamma/\pi}\, M\,\mathrm{Kn}$),

$$\frac{u^*}{u^*(0)} = 1 - \frac{T_w^{*2}}{2u^*(0)} \frac{\varepsilon_{h_w}}{N_\delta} \cdot \left( \frac{\tan S^*}{2S^*_{1/2}} \right)^2. \tag{8}$$

The NCCR solution for the temperature profile is then given as

$$\frac{T^*}{T^*(0)} = \cos^{-e} S^* \left(1 - \frac{\pi(\gamma-1)\,\mathrm{Pr}}{24\gamma(1-e/4)} \frac{T_w^{*5}}{T^*(0)} \frac{\varepsilon_{h_w}^2}{\mathrm{Kn}^2} \frac{F(S^*)}{(2S_{1/2}^*)^4}\right), \tag{9}$$

where $e = 3(\gamma-1)/(2\gamma)$, $ds \equiv dy/T$, $y^* \equiv y/h$, $S^* \equiv \sqrt{2/3} T_w^* \varepsilon_{h_w} s^*$, and $s^* \equiv sT_r/h$. Here the trigonometric function $F$ is defined as

$$F(t) \equiv (4-e)\left[\frac{1}{(4-e)\cos^{4-e} t} - \frac{1}{(2-e)\cos^{2-e} t} - \left(\frac{1}{4-e} - \frac{1}{2-e}\right)\right].$$

The velocity and temperature were made dimensionless by using the following unknown average properties:

$$u_r = \frac{2}{h}\int_0^{h/2} u dy,\; T_r = \frac{h/2}{\int_0^{h/2} 1/T dy}.$$

Note that the function $F$ is related to the *quartic* function in the classical NSF solution as follows:

$$F(t) = \left(1 - \frac{e}{4}\right) t^4 + O(t^6).$$

On the other hand, the factor in the temperature solution $\cos^{-e} t$, directly related to the force parameter $\varepsilon_{h_w}$, is basically *quadratic* since

$$\cos^{-e}(t) = 1 + \frac{e}{2} t^2 + O(t^4),$$

and it is responsible for the central temperature minimum. The unknown value $T_w^*$ in (8), that is, the average temperature, can be determined uniquely for any given values of Kn and $\varepsilon_{h_w}$ by solving the following algebraic equation using the bisection method:

$$\begin{aligned} &\frac{\pi(\gamma-1)\,\mathrm{Pr}\,\varepsilon_{h_w}^2 T_w^{*5}}{384\gamma \mathrm{Kn}^2(1-e/4)} \frac{F(S_{1/2}^*)}{S_{1/2}^{*4}} = T^*(0)\left(1 - (1-\alpha_T)\sec^{-e} S_{1/2}^*\right) - \alpha_T T_w^* \sec^{-e} S_{1/2}^*, \\ &\alpha_T = \frac{\bar{\beta}_T p_w^*}{1 + \bar{\beta}_T p_w^*},\; \bar{\beta}_T = \frac{1}{4\omega_T \mathrm{Kn}}. \end{aligned} \tag{10}$$

Here the $\omega_T$ is the temperature jump coefficient[10,21] defined as $(2-\phi_T)/\phi_T$, where $\phi_T$ is the energy accommodation coefficient, and is assumed to be 1.

The NCCR solutions for pressure and shear and normal stresses are given by ($\Pi_{yy} = \Pi_{zz} = -\Pi_{xx}/2$)

$$\begin{aligned} &p^*(S^*) = 1 + \tan^2 S^*, \\ &\left[\Pi_{xy}^*(S^*)\right]_0 = \frac{1}{N_\delta}\sqrt{\frac{3}{2}} \tan S^*,\; \left[\Pi_{yy}^*(S^*)\right]_0 = -\frac{1}{N_\delta}\tan^2 S^*. \end{aligned} \tag{11}$$

An abbreviation $[A]_0 \equiv A - A(0)$ is introduced to represent the value of a quantity $A$ measured from its value at the center, that is, $A(0)$. The solutions are a function of tangent and show the central minimum in pressure. Note that the slip (jump) boundary conditions play an indirect role at negligible levels in pressure and stresses, only through the determination of average temperature $T_w^*$. The tangent functional forms in pressure and stresses hold for any monatomic gases. Further, the density distribution across the channel is calculated using the equation of state,

$$\rho^*(s^*) = T^*(0)\frac{p^*}{T^*}. \tag{12}$$

Finally, the NCCR solutions for normal and tangential heat fluxes can be expressed as, respectively,

$$\begin{aligned} &\left[Q_y^*\right]_0 = \frac{1}{3}\,\mathrm{Pr}\,\mathrm{Ec} T_w^{*3} \frac{\varepsilon_{h_w}^2}{N_\delta^2}\left(\frac{\tan S^*}{2S_{1/2}^*}\right)^3, \\ &\left[Q_x^*\right]_0 = N_\delta\left[\left(1 + \frac{1}{\mathrm{Pr}}\right)\left[\Pi_{xy}^*\right]_0\left[Q_y^*\right]_0 - \varepsilon_{h_w}\frac{T_r}{\Delta T}\frac{(\gamma-1)}{\gamma}\frac{T^*}{p^*}\left(2\left[\Pi_{yy}^*\right]_0 + N_\delta\left[\Pi_{xy}^*\right]_0^2\right)\right]. \end{aligned} \tag{13}$$

On the other hand, the second-order NCCR solutions (8)-(13) are reduced to the first-order compressible NSF solutions (the conservation laws in conjunction with the linear NSF laws (2)) near thermal equilibrium as follows; in order of velocity, temperature, pressure, viscous stresses, density, and heat fluxes,

$$\begin{aligned}
&\frac{u^*}{u^*(0)} = 1 - \frac{T_w^{*2}}{2u^*(0)}\frac{\varepsilon_{h_w}}{N_\delta}s^{*2},\\
&\frac{T^*}{T^*(0)} = 1 - \frac{\pi(\gamma-1)\,\mathrm{Pr}}{24\gamma}\frac{T_w^{*5}}{T^*(0)}\frac{\varepsilon_{h_w}^2}{\mathrm{Kn}^2}s^{*4},\ \text{where}\ \frac{\pi(\gamma-1)\,\mathrm{Pr}\,\varepsilon_{h_w}^2 T_w^{*5}}{384\gamma\mathrm{Kn}^2} = \frac{5\alpha_T}{5-\alpha_T}(1-T_w^*),\\
&p^*(s^*) = 1,\ \left[\Pi_{xy}^*(s^*)\right]_0 = T_w^*\frac{\varepsilon_{h_w}}{N_\delta}s^*,\ \left[\Pi_{yy}^*(s^*)\right]_0 = 0,\\
&\rho^*(s^*) = T^*(0)\frac{p^*}{T^*},\\
&\left[Q_y^*\right]_0 = \frac{1}{3}\,\mathrm{Pr}\,\mathrm{Ec}T_w^{*3}\frac{\varepsilon_{h_w}^2}{N_\delta^2}s^{*3},\ \left[Q_x^*\right]_0 = 0.
\end{aligned} \tag{14}$$

(The detailed information of the analytical NSF solutions is available in the work of Myong.[10])

## III. ATOMIC-LEVEL MD SIMULATION SETUP

The force-driven Poiseuille flow in the present MD simulation is described using argon as fluid atoms constrained between platinum wall atoms. The walls are separated by $L = 100$ Å, parallel to the $x$-$z$ plane. Initially, all wall atoms, with mass $m_{\mathrm{Pt}} = 195.08$ g/mol and diameter $d_{\mathrm{Pt}} = 2.77$ Å, are arranged in six layers each with a face-centered cubic (FCC) lattice, with a lattice constant of 3.92 Å. The interaction between the fluid and wall atoms are modeled by Lennard-Jones (LJ) shifted force potential with the cutoff distance as $2.5\sigma$. The LJ interaction parameters for argon fluid and platinum wall atoms are $\sigma_{\mathrm{Ar}} = 3.4$ Å, $\varepsilon_{\mathrm{Ar}} = 0.238\,18$ kcal/mol, $\sigma_{\mathrm{Pt}} = 2.47$ Å, $\varepsilon_{\mathrm{Pt}} = 7.4981$ kcal/mol, respectively.[22] The LJ parameters to model the interaction between fluid and wall atoms are calculated by the Lorentz-Berthelot mixing rule[23] as $\sigma_{\mathrm{Pt-Ar}} = 2.935$ Å, $\varepsilon_{\mathrm{Pt-Ar}} = 1.5739$ kcal/mol.

The flow is generated by an external constant force $F_x$ (kcal/mol Å) applied uniformly on each atom in the $x$-direction, as illustrated in Fig. 2. The heat flux due to fluid friction is dissipated through the walls by maintaining the walls at constant temperature (300 K) by Berendsen thermostat.[24] The channel dimension is $98 \times 100 \times 98$ Å$^3$ and the simulation domain is periodic in all three dimensions, similar to the method adopted in Ref. 22. To eliminate the interactions between the two walls due to periodicity, some empty space is provided beyond the walls. The calculations were

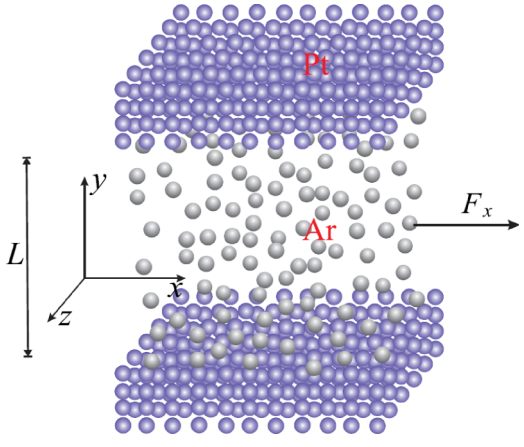


FIG. 2. MD simulation setup of the Poiseuille gas flow between two walls. The fluid atoms are driven by a force applied uniformly in the $x$-direction.

performed for $70 \times 10^6$ time steps with a time step of 1 fs. The integrations were performed using the velocity-Verlet algorithm in a microcanonical (NVE) ensemble.

In the post-processing of the MD simulation data, average results across the channel were obtained by dividing the channel into a number of equally divided bins. The binned values were then time-averaged for a number of time steps. The properties were averaged for all the atoms in each bin, which resulted in a representative value for that bin. The spatial averaging was performed across the channel by binning method[25] with 80 bins. It was observed that the simulation reaches the steady state after the first $20 \times 10^6$ of time steps. Therefore, the properties were averaged for the last $50 \times 10^6$ steps, after the system has reached the steady state. The density in each bin was then obtained by counting the mass of the total number of atoms. Finally, the pressure and stress tensor and heat flux vector were calculated by the Irving-Kirkwood procedure.[25] The calculation of the pressure and non-conserved variables (in particular, normal viscous stress and tangential heat flux) directly from the molecular data using the statistical method turned out to be extremely important, since it is not possible to validate the constitutive laws without information of the viscous stress and heat flux. The simulations were performed using the open source MD simulation package LAMMPS (Large-scale Atomic/Molecular Massively Parallel Simulator) distributed by Sandia National Laboratories.[26]

## IV. MD CHARACTERIZATION OF THE SECOND-ORDER NON-NAVIER-FOURIER CONSTITUTIVE LAWS

In the present simulation, the total number of gas atoms, 1470, in a $L \times L \times L$ volume was considered, yielding a Knudsen number Kn = 0.1 in the transition regime. A constant force, $a(= F_x) = 3.575 \times 10^{-3}$ kcal/mol Å, was applied uniformly on each atom, leading to a force parameter $\varepsilon_{h_w} = 0.6$. The results obtained from the MD simulation were compared with the compressible NSF solution,[10] the second-order non-Navier-Fourier solutions based on the NCCR theory summarized in Section II, and DSMC data for a hard sphere gas obtained by Uribe and Garcia.[6] Among various direct solutions of the Boltzmann equation, the DSMC data by Uribe and Garcia were chosen because the pressure, normal viscous stress, and tangential heat flux, all of which are essential in validating the non-classical constitutive laws, are available. Under the present flow conditions, it was shown by previous work[10] that the flow within the channel is high subsonic, having average Mach numbers of $M = 0.679\,15$ and $0.706\,53$, according to the compressible NSF and NCCR theories, respectively.[10]

### A. Conserved properties and the case of pressure near wall

The conserved properties of MD simulation are depicted in Figs. 3-6. The MD density data are in qualitative agreement with NCCR and DSMC data, as shown in Fig. 3. Here the properties are

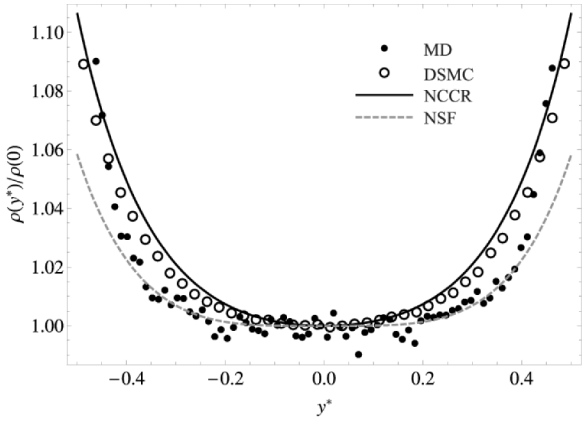


FIG. 3. Density distribution $\rho(y^*)/\rho(0)$ in the force-driven compressible Poiseuille gas flow ($\varepsilon_{h_w} = 0.6$, Kn = 0.1).

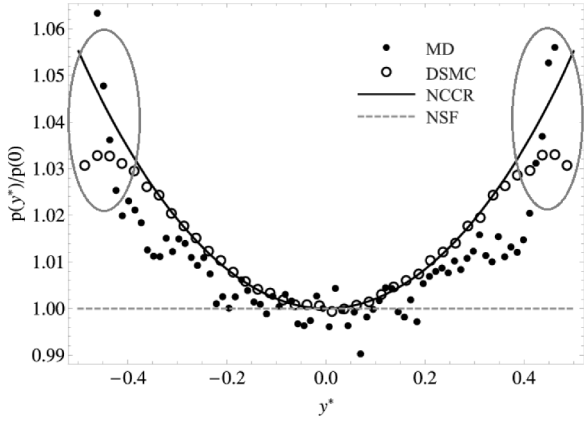


FIG. 4. Pressure distribution $p(y^*)/p(0)$ in the force-driven compressible Poiseuille gas flow ($\varepsilon_{h_w} = 0.6$, Kn = 0.1).

non-dimensionalized with respect to the values at the centerline, while the location in the channel is non-dimensionalized with the channel height. In general, all data, including the classical NSF theory, predict essentially the same trend: minimum at the center and maximum at the wall. This finding is not surprising since any theory based on the conservation law of mass, whether classical or non-classical, will share the same qualitative behavior. The reason is that the conservation law of mass is automatically satisfied in the case of one-dimensional Poiseuille flow problem, due to the simple non-locality relation, $v = 0, \partial/\partial x = 0$, imposing no restriction on the density.

Nonetheless, there is a substantial gap in the case of the classical NSF theory, in particular, near the wall. The cause of this disparity can be easily identified from Fig. 4 of the pressure profile, in which only the classical NSF theory predicts constant pressure, while all other results show the non-uniform (quadratic) convex pressure profile with a maximum near the wall; for instance, $1 + \tan^2(\sqrt{2/3}T_w^*\varepsilon_{h_w}s^*)$ for the second-order NCCR theory. This difference causes the density of the classical theory to be lower than that of other non-classical data, through the equation of state (12). On the other hand, the ultimate origin of the non-uniform pressure profile can be explained from the kinematic stress constraint given in (3) and the $y$-momentum equation of the conservation law $p + \Pi_{yy} = p(0)$; that is, non-zero shear stress generated by the external force induces non-zero normal stress which in turn causes non-uniform pressure profile. The peculiar nature of the force-driven Poiseuille flow — the appearance of the forcing term $\rho a$ in the $x$-momentum equation of the conservation laws $d\Pi_{xy}/dy = \rho a$ — causes the stress constraint to stand out unexpectedly in the transition regime.

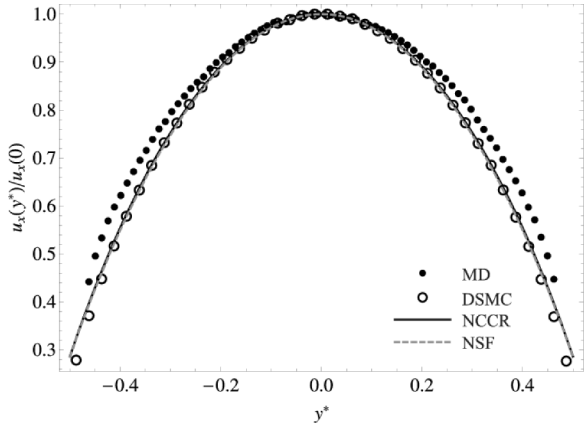


FIG. 5. Velocity distribution $u(y^*)/u(0)$ in the force-driven compressible Poiseuille gas flow ($\varepsilon_{h_w} = 0.6$, Kn = 0.1).

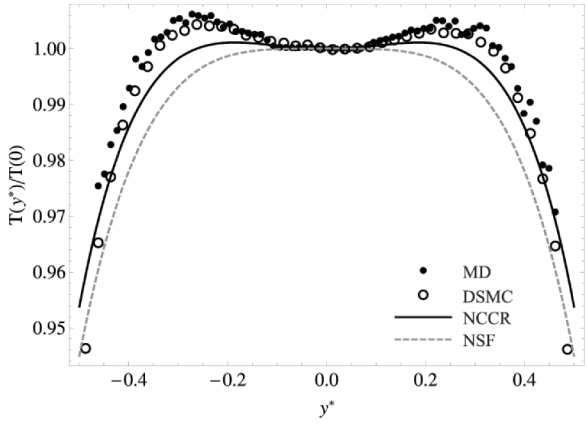


FIG. 6. Temperature distribution $T(y^*)/T(0)$ in the force-driven compressible Poiseuille gas flow ($\varepsilon_{h_w} = 0.6$, Kn = 0.1).

Fig. 4 of pressure profile also shows a very interesting point that the DSMC solution shows unusual behavior of increase and decrease near the wall, while the MD result and the second-order NCCR theory ($1 + \tan^2 S^*$) show *strict monotonic increase*. As shown recently by Karchani and Myong in an analysis of error estimation of the DSMC in the compressible velocity-shear dominated Couette flow based on the physical laws of conservation [Ref. 27 in Fig. 5], this DSMC behavior may be explained that the DSMC solution near the wall was contaminated by computational errors associated with the gas-wall interaction. The reason is that it is improbable to think that only the pressure (very resilient property) profile suddenly changes its qualitative behavior near the wall, from monotonic to non-monotonic, when all other (conserved) thermodynamic properties (density and temperature) remain strictly monotonic. This may indicate that the current *mesoscopic* DSMC (in which one simulation particle represents real molecules in order of $10^{6-13}$) has a limitation in validating the properties near the wall in fundamental level and deterministic *atomic-level microscopic* MD simulation is required to complement the validation study.

Figs. 5 and 6 depict the remaining conserved variables (streamwise velocity and temperature). For velocity, all data including the MD simulation predict essentially the same trend: a quadratic profile with a maximum at the center. However, there is a fundamental difference in the temperature profile: a maximum at the center in the classical NSF theory, although a minimum at the center in the non-classical results (NCCR theory, DSMC, and MD data). According to the analytical NCCR theory, the ultimate source of the central temperature minimum can be traced to the extra coupling term of viscous shear stress and force, $a\Pi_{xy}$, appearing in the non-Fourier law of heat flux given in (4). The coupling term then gives rise to the factor $\cos^{-e} S^*$ in the non-classical solution of temperature (9) and makes the profile quadratic near the center, in contrast with pure quartic in the classical solution.

### B. Non-conserved properties for the second-order constitutive laws and phase portraits

Figs. 7-10 depict the non-conserved variables (shear stress, normal stresses, normal heat flux, and tangential heat flux) measured from the values at the center. For shear stress and normal heat flux, all the data including the MD simulation show essentially the same qualitative behaviors. However, only the non-classical results (NCCR, DSMC, and MD) can correctly describe the existence of non-zero normal stress and tangential heat flux, while the classical NSF theory misses them completely. Again, the ultimate origin of these abnormal behaviors can be explained in concise way by the non-classical non-Navier-Fourier laws (3) and (4) of the second-order NCCR theory (equivalently, the analytical solutions (11) and (13)). Notice that the normal stress profile $\Pi^*_{yy}(S^*)$ is quadratic near the center through $\tan^2 S^*$ of (11), while the tangential heat flux profile $Q^*_x(S^*)$ is quartic near the center through $\tan^4 S^*$ of (13), since it is proportional to $\Pi^*_{xy} Q^*_y$. Both are convincingly validated by the MD and DSMC simulation data.

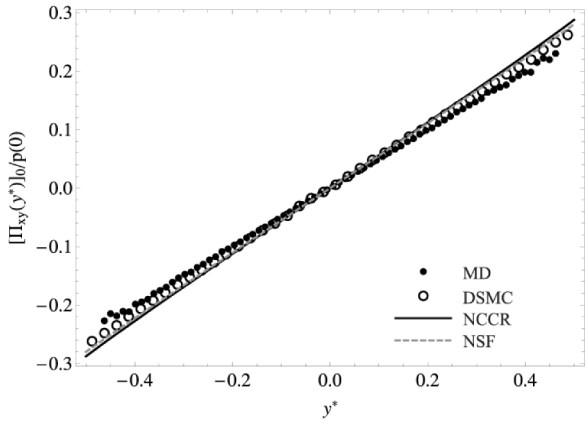


FIG. 7. Shear stress distribution $[\Pi_{xy}(y^*)]_0/p(0)$ in the force-driven compressible Poiseuille gas flow ($\varepsilon_{h_w} = 0.6$, Kn = 0.1).

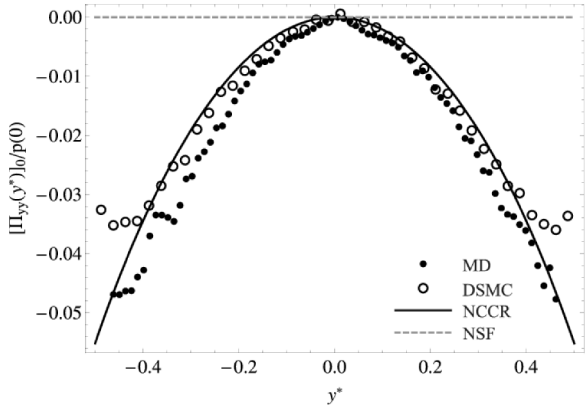


FIG. 8. Normal stress distribution $[\Pi_{yy}(y^*)]_0/p(0)$ in the force-driven compressible Poiseuille gas flow ($\varepsilon_{h_w} = 0.6$, Kn = 0.1).

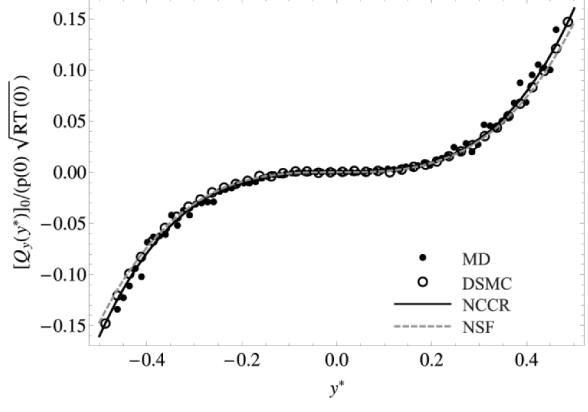


FIG. 9. Normal heat flux distribution $[Q_y(y^*)]_0/\left(p(0)\sqrt{RT(0)}\right)$ in the force-driven compressible Poiseuille gas flow ($\varepsilon_{h_w} = 0.6$, Kn = 0.1).

In Figs. 11 and 12, the phase portraits of stress and heat flux are depicted in order to confirm the existence of the constraints on stress and heat flux given in (3) and (4). The stress and heat flux are normalized by the pressure $p$ and a reference value $p(0)\sqrt{RT(0)}$, respectively. All non-classical results (NCCR, DSMC, and MD) clearly show the existence of the constraints of stress (quadratic) and heat flux (linear), while the classical NSF theory describes none of them.

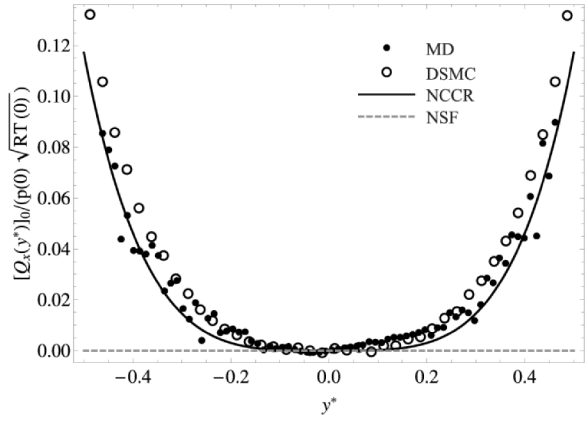


FIG. 10. Tangential heat flux distribution $\left[Q_y(y^*)\right]_0/\left(p(0)\sqrt{RT(0)}\right)$ in the force-driven compressible Poiseuille gas flow ($\varepsilon_{h_w} = 0.6$, Kn = 0.1).

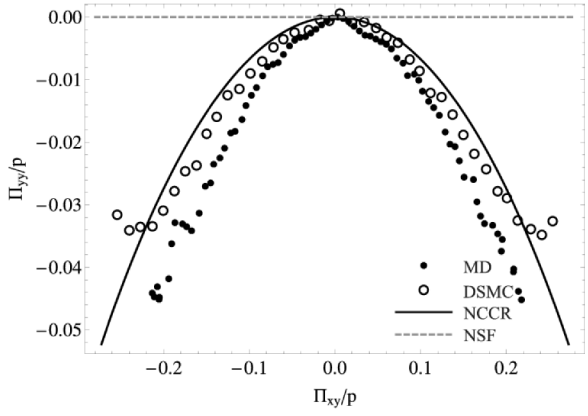


FIG. 11. Kinematic constraint on viscous stresses $\left[\Pi_{xy}\right]_0/p$ vs $\left[\Pi_{yy}\right]_0/p$ for $-1/2 < y^* < 1/2$ in the force-driven compressible Poiseuille gas flow ($\varepsilon_{h_w} = 0.6$, Kn = 0.1).

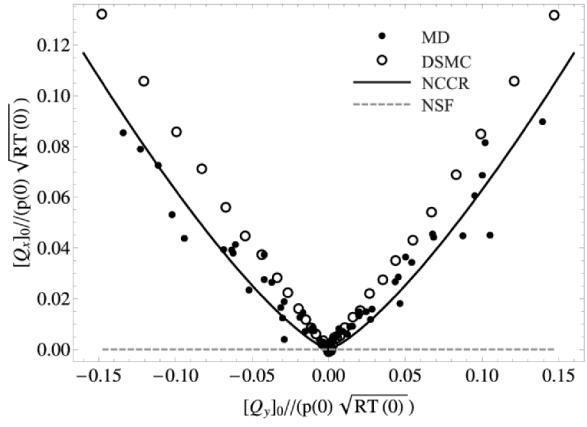


FIG. 12. Relationship between heat fluxes $\left[Q_{y,x}(y^*)\right]_0/\left(p(0)\sqrt{RT(0)}\right)$ for $-1/2 < y^* < 1/2$ in the force-driven compressible Poiseuille gas flow ($\varepsilon_{h_w} = 0.6$, Kn = 0.1).

### C. Validation of the second-order non-Navier-Fourier constitutive laws and theory behind exotic heat conduction from cold to hot

Finally, in order to validate the second-order non-Navier-Fourier constitutive laws (3) and (4), the non-conserved variables are depicted with respect to the thermodynamic forces (that is, the

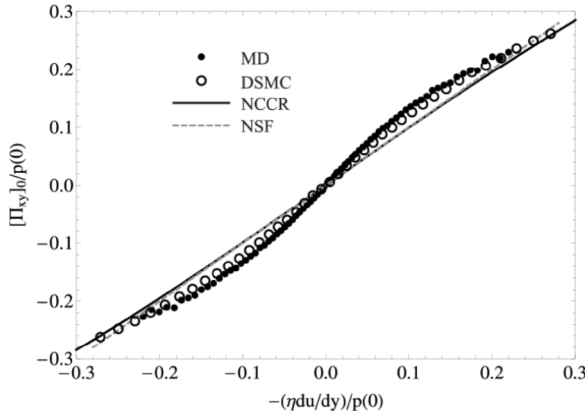


FIG. 13. Shear stress in function of the velocity gradient $-\eta du/dy/p(0)$ vs $\left[\Pi_{xy}(y^*)\right]_0/p(0)$ in the force-driven compressible Poiseuille gas flow ($\varepsilon_{h_w} = 0.6$, Kn = 0.1).

gradients of velocity and temperature for stress and heat flux, respectively) in Figs. 13-16. For shear stress in Fig. 13, all results, including the MD simulation, show essentially the same property close to the linear law in the transition regime. However, as was already observed in Fig. 8 for normal stress, there is a fundamental difference in the case of normal stress in Fig. 14: zero in classical NSF theory, whereas non-zero and quadratic in the non-classical results (NCCR theory, DSMC, and MD data). A similar conclusion can be found for the normal and tangential heat fluxes as shown in Figs. 15 and 16. In the case of normal heat flux, all results including the MD simulation show essentially the same property, almost linear law in the transition regime. In addition, the tangential heat flux is strictly zero in the case of the classical NSF theory, while it remains non-zero and linear in the non-classical results.

On the other hand, there is a very interesting phenomenon directly related to the central temperature minimum in the case of heat flux. When the central temperature minimum in Fig. 6 is carefully examined in conjunction with the normal heat flux distribution in Fig. 9, it can be observed that the central region shows instantaneous heat conduction from the cold region to the hot region, which seems completely odd, at first glance, and against the conventional Fourier law. In fact, such an exotic non-Fourier law is highlighted in the zoomed boxes of Figs. 15 and 16. When the temperature increases in the positive $y$-direction near the center, the normal heat flux according to the non-Fourier law (4) becomes positive, while it remains strictly negative in the conventional Fourier law, $Q_{y_0} = -kdT/dy$. This fundamental behavior leads to the existence of the exotic non-Fourier constitutive law near the center in the force-driven Poiseuille flow. Similarly, the odd-looking

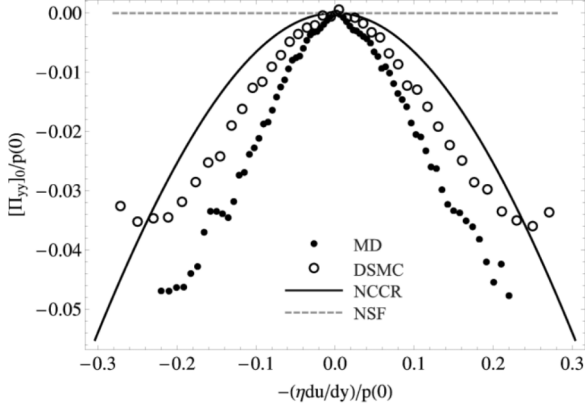


FIG. 14. Normal stress in function of the velocity gradient $-\eta du/dy/p(0)$ vs $\left[\Pi_{yy}(y^*)\right]_0/p(0)$ in the force-driven compressible Poiseuille gas flow ($\varepsilon_{h_w} = 0.6$, Kn = 0.1).

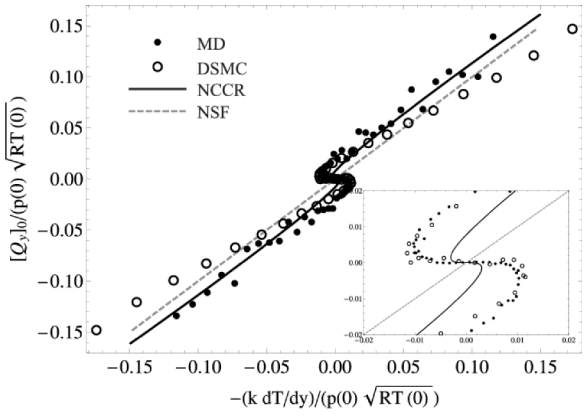


FIG. 15. Normal heat flux in function of the temperature gradient $-k\,dT/dy/\left(p(0)\sqrt{RT(0)}\right)$ vs $[Q_y(y^*)]_0/\left(p(0)\sqrt{RT(0)}\right)$ in the force-driven compressible Poiseuille gas flow ($\varepsilon_{h_w} = 0.6$, Kn = 0.1).

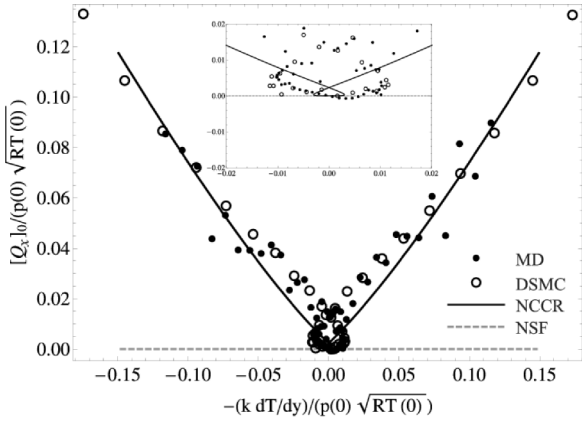


FIG. 16. Tangential heat flux in function of the temperature gradient $-k\,dT/dy/\left(p(0)\sqrt{RT(0)}\right)$ vs $[Q_x(y^*)]_0/\left(p(0)\sqrt{RT(0)}\right)$ in the force-driven compressible Poiseuille gas flow ($\varepsilon_{h_w} = 0.6$, Kn = 0.1).

behavior near the origin observed from the zoomed box of Fig. 16 of tangential heat flux can be explained by the exotic heat conduction from cold to hot.

In summary, after having validated various non-classical phenomena, in particular, the pressure and non-conserved variables (normal viscous stress and tangential heat flux), using the deterministic atomic-level microscopic MD simulation, it would be safe to conclude that the algebraic second-order non-Navier-Fourier constitutive laws (3) and (4) deduced from the second-order exact consequence of the Boltzmann equation (1) are physically legitimate in velocity shear flows.

## V. CONCLUSION

The second-order non-Navier-Fourier constitutive laws, expressed in a compact algebraic mathematical form, were for the first time validated for the force-driven Poiseuille gas flow by the deterministic atomic-level microscopic MD. Emphasis was placed on how three completely different methods (a *second-order continuum* macroscopic NCCR theory based on the kinetic Boltzmann equation, the *probabilistic* mesoscopic DSMC, and, in particular, the *deterministic* microscopic MD) describe the non-classical physics, and whether the second-order non-Navier-Fourier constitutive laws derived from the NCCR theory could be validated using MD solutions for the viscous stress and heat flux calculated directly from the molecular data using the statistical method like the Irving-Kirkwood procedure.

It was shown that all the results obtained by the three methods were in strong qualitative agreement with each other. The level of agreement is higher than expected, considering the uncertainties that may arise from different types of gas (Maxwellian molecule, hard sphere, and argon atom), and different treatments of the gas-wall molecular interaction (accommodation coefficient, diffusive interaction, and Lennard-Jones interaction parameter). Also, a mathematical simplification $q_{2nd}(\kappa) \approx 1$ was introduced to the NCCR theory on the ground that the $\sinh \kappa/\kappa$ term may play a negligible role in velocity shear flow. Therefore, the fair agreement between the NCCR theory and the MD and DSMC data may imply that the second-order non-Navier-Fourier constitutive laws expressed as a compact algebraic mathematical form (3) and (4) are indeed physically legitimate in the transition regime.

Nonetheless, a gap between the DSMC and the MD-NCCR in the pressure profile near the wall, *non-monotonic* versus *strict monotonic*, was also identified. It is suspected that the DSMC solution near the wall was contaminated by computational errors associated with the gas-wall interaction. This finding may indicate that the current mesoscopic DSMC has a limitation in validating the higher-order constitutive laws near the wall in fundamental level and deterministic atomic-level microscopic MD simulation is required to complement the validation study.

Furthermore, it was shown that there is a fundamental difference in the role of non-classical laws in the transition regime. The plots of the non-conserved variables with respect to the thermodynamic forces indicated that the non-Navier-Fourier laws are essential in describing non-zero normal stress and tangential heat flux, while the classical and non-classical laws remain similar (linear) for shear stress and normal heat flux.

Overall, the present study demonstrated that non-classical thermal physics arising from the second-order non-Navier-Fourier constitutive laws play an essential role in flows far from thermal equilibrium and consequently thermal aspects must be treated fully. Even with an isothermal wall condition, an exotic temperature profile can be formed by the non-Fourier law and it may result in abnormal behaviors, like the Knudsen minimum in mass flow rate and the instantaneous heat conduction from cold to hot. Therefore, theoretical and experimental investigations of the whole flow fields, like cross-stream pressure and temperature, and heat flux distributions beyond the usual reduced quantities like the mass flow rate, will remain essential for obtaining a deeper understanding of rarefied and micro- and nano-scale gas flows.

## ACKNOWLEDGMENTS

This work was supported by the National Research Foundation of Korea funded by the Ministry of Education, Science and Technology (Grant No. NRF 2015-M1A3A3A02-010621), South Korea.

[1] J. M. Reese, M. A. Gallis, and D. A. Lockerby, "New directions in fluid dynamics: Non-equilibrium aerodynamic and microsystem flows," Philos. Trans. R. Soc., A **361**, 2967 (2003).
[2] D. J. Alofs and G. S. Springer, "Cylindrical Couette flow experiments in the transition regime," Phys. Fluids **14**(2), 298 (1971).
[3] M. Rojas-Cárdenas, I. Graur, P. Perrier, and J. G. Méolans, "A new method to measure the thermal slip coefficient," Int. J. Heat Mass Transfer **88**, 766 (2015).
[4] F. Samouda, S. Colin, C. Barrot, L. Baldas, and J. J. Brandner, "Micro molecular tagging velocimetry for analysis of gas flows in mini and micro systems," Microsyst. Technol. **21**(3), 527 (2015).
[5] M. M. Mansour, F. Baras, and A. L. Garcia, "On the validity of hydrodynamics in plane Poiseuille Flows," Physica A **240**, 255 (1997).
[6] F. J. Uribe and A. L. Garcia, "Burnett description of plane Poiseuille flow," Phys. Rev. E **60**, 4063 (1999).
[7] Y. Zheng, A. L. Garcia, and B. J. Alder, "Comparison of kinetic theory and hydrodynamics for Poiseuille flow," J. Stat. Phys. **109**(3/4), 495 (2002).
[8] K. Xu, "Super-Burnett solutions for Poiseuille flow," Phys. Fluids **15**(7), 2077 (2003).
[9] P. Taheri, M. Torrilhon, and H. Struchtrup, "Couette and Poiseuille microflows: Analytical solutions for regularized 13-moment equations," Phys. Fluids **21**(1), 017102 (2009).
[10] R. S. Myong, "A full analytical solution for the force-driven compressible Poiseuille gas flow based on a nonlinear coupled constitutive relation," Phys. Fluids **23**(1), 012002 (2011), http://acml.gnu.ac.kr.
[11] L. Wu, C. White, T. J. Scanlon, J. M. Reese, and Y. Zhang, "Deterministic numerical solutions of the Boltzmann equation using the fast spectral method," J. Comput. Phys. **250**, 27 (2013).
[12] C. L. M. H. Navier, "Mémoire sur les lois du movement des fluids," Mém. Acad. Sci. Inst. France **6**, 375 (1822).
[13] J. B. J. Fourier, *Théorie Analytique de la Chaleur* (Chez Firmin Didot, Paris, 1822).

[14] R. S. Myong, "On the high Mach number shock structure singularity caused by overreach of Maxwellian molecules," Phys. Fluids **26**(5), 056102 (2014).
[15] R. S. Myong, "Theoretical description of the gaseous Knudsen layer in Couette flow based on the second-order constitutive and slip-jump models," Phys. Fluids **28**(1), 012002 (2016).
[16] B. C. Eu, "A modified moment method and irreversible thermodynamics," J. Chem. Phys. **73**, 2958 (1980).
[17] B. C. Eu, *Kinetic Theory and Irreversible Thermodynamics* (Wiley, New York, 1992).
[18] L. Hannon, G. C. Lie, and E. Clementi, "Molecular dynamics simulation of channel flow," Phys. Lett. A **119**(4), 174 (1986).
[19] D. K. Bhattacharya and G. C. Lie, "Molecular-dynamics simulations of nonequilibrium heat and momentum transport in very dilute gases," Phys. Rev. Lett. **62**(8), 897 (1989).
[20] B. D. Todd and D. J. Evans, "Temperature profile for Poiseuille flow," Phys. Rev. E **55**(3), 2800 (1997).
[21] R. S. Myong, "Gaseous slip model based on the Langmuir adsorption isotherm," Phys. Fluids **16**(1), 104 (2004).
[22] S. K. Prabha and S. P. Sathian, "Molecular-dynamics study of Poiseuille flow in a nanochannel and calculation of energy and momentum accommodation coefficients," Phys. Rev. E **85**(4), 041201 (2012).
[23] M. P. Allen and D. J. Tildesley, *Computer Simulation of Liquids* (Clarendon, Oxford, 1987).
[24] H. J. C. Berendsen, J. P. M. Postma, W. F. van Gunsteren, A. DiNola, and J. R. Haak, "Molecular dynamics with coupling to an external bath," J. Chem. Phys. **81**, 3684 (1984).
[25] J. H. Irving and J. G. Kirkwood, "The statistical mechanical theory of transport processes. IV. The equations of hydrodynamics," J. Chem. Phys. **18**, 817 (1950).
[26] S. Plimpton, "Fast parallel algorithms for short-range molecular dynamics," J. Comput. Phys. **117**, 1 (1995), http://lammps.sandia.gov.
[27] A. Karchani and R. S. Myong, "Convergence analysis of the direct simulation Monte Carlo based on the physical laws of conservation," Comput. Fluids **115**, 98 (2015).